A robust and active hybrid catalyst for facile oxygen reduction in solid oxide fuel cells

Citation: Chen, Yu et al. "A Robust and Active Hybrid Catalyst for Facile Oxygen Reduction in Solid Oxide Fuel Cells." Energy & Environmental Science 10, 4 (2017): 964–971 © 2017 The Royal Society of Chemistry

As Published: http://dx.doi.org/10.1039/C6EE03656B

Publisher: Royal Society of Chemistry (RSC)

Persistent URL: http://hdl.handle.net/1721.1/117088

Version: Author's final manuscript: final author's manuscript post peer review, without publisher's formatting or copy editing

Energy & Environmental Science

PAPER

View Article Online
View Journal

Cite this: DOI: 10.1039/c6ee03656b

A robust and active hybrid catalyst for facile oxygen reduction in solid oxide fuel cells†

Yu Chen,‡[a] Yan Chen,‡[bc] Dong Ding,‡[a] Yong Ding,[a] YongMan Choi,[d] Lei Zhang,[a] Seonyoung Yoo,[a] Dongchang Chen,[a] Ben deGlee,[a] Han Xu,[a] Qiyang Lu,[b] Bote Zhao,[a] Gulin Vardar,[b] Jiayue Wang,[b] Hendrik Bluhm,[e] Ethan J. Crumlin,[e] Chenghao Yang,[c] Jiang Liu,[c] Bilge Yildiz*[b] and Meilin Liu*[a]

Received 17th December 2016,
Accepted 13th March 2017

DOI: 10.1039/c6ee03656b

rsc.li/ees

The sluggish oxygen reduction reaction (ORR) greatly reduces the energy efficiency of solid oxide fuel cells (SOFCs). Here we report our findings in dramatically enhancing the ORR kinetics and durability of the state-of-the-art $La_{0.6}Sr_{0.4}Co_{0.2}Fe_{0.8}O_3$ (LSCF) cathode using a hybrid catalyst coating composed of a conformal $PrNi_{0.5}Mn_{0.5}O_3$ (PNM) thin film with exsoluted PrO_x nanoparticles. At 750 °C, the hybrid catalyst-coated LSCF cathode shows a polarization resistance of ~0.022 Ω cm^2, about 1/6 of that for a bare LSCF cathode (~0.134 Ω cm^2). Further, anode-supported cells with the hybrid catalyst-coated LSCF cathode demonstrate remarkable peak power densities (~1.21 W cm^{-2}) while maintaining excellent durability (0.7 V for ~500 h). Near Ambient X-ray Photoelectron Spectroscopy (XPS) and Near Edge X-Ray Absorption Fine Structure (NEXAFS) analyses, together with density functional theory (DFT) calculations, indicate that the oxygen-vacancy-rich surfaces of the PrO_x nanoparticles greatly accelerate the rate of electron transfer in the ORR whereas the thin PNM film facilitates rapid oxide-ion transport while drastically enhancing the surface stability of the LSCF electrode.

Broader context

Intermediate-temperature solid oxide fuel cells (IT-SOFCs) have the potential to be the cleanest and most efficient options for cost-effective utilization of a wide variety of fuels, from hydrogen to hydrocarbons, coal gas, and renewable fuels. They are ideally suited for distributed generation (which may be integrated with smart grids) and for mobile applications (*e.g.*, electric vehicles). To make IT-SOFCs economically competitive and commercially viable, however, several material challenges must be overcome. One of them is the creation of durable, low-cost cathode materials and nanostructures of high electro-catalytic activity for the oxygen reduction reaction (ORR) at intermediate temperatures. Here we report an effective strategy for the fabrication of high-performance hybrid catalyst coated electrodes with dramatically enhanced ORR activity and durability for fuel cells. The concept of surface modification of electrodes through solution-infiltration of a catalyst and the unique hybrid electrode structure (exsoluted nanoparticles on a conformal coating) are readily applicable to other energy storage and conversion systems, including metal–air batteries, supercapacitors, electrolyzers, dye-sensitized solar cells, and photo-catalysis.

Introduction

The demand for clean, secure, and economically competitive energy has stimulated great interest in fuel cells for efficient energy conversion.[1–4] Among all types of fuel cells, solid oxide fuel cells (SOFCs) are the cleanest, most efficient chemical-to-electrical energy conversion systems with excellent fuel flexibility.[5–8] However, broad commercialization of SOFC technology is still hampered by high cost and limited system lifetimes.[9] The resistance from the oxygen reduction reaction (ORR) contributes the most to energy loss in the existing SOFCs, more so at lower temperatures.[10–12] Therefore, a key technical opportunity is to dramatically enhance the ORR kinetics and durability of the cathode at low temperatures.

[a] *Materials Science and Engineering, Georgia Institute of Technology, Atlanta, GA 30332-0245, USA. E-mail: meilin.liu@mse.gatech.edu*
[b] *Laboratory for Electrochemical Interfaces, Department of Nuclear Science and Engineering and Department of Materials Science and Engineering, Massachusetts Institute of Technology, 77 Massachusetts Avenue, Cambridge, MA 02139, USA. E-mail: byildiz@mit.edu*
[c] *Guangzhou Key Laboratory for Surface Chemistry of Energy Materials, New Energy Research Institute, School of Environment and Energy South China University of Technology, Guangzhou 510006, China*
[d] *SABIC Technology Center, Riyadh 11551, Saudi Arabia*
[e] *Advanced Light Source, Lawrence Berkeley National Laboratory, Berkeley, California 94720, USA*

† Electronic supplementary information (ESI) available. See DOI: 10.1039/c6ee03656b

‡ These authors contributed equally to this work.

As one of the most promising cathode candidates for intermediate-temperature SOFCs, $La_{0.6}Sr_{0.4}Co_{0.2}Fe_{0.8}O_3$ (LSCF) has been extensively investigated because of its high electronic and ionic conductivities and good catalytic activity for the ORR. However, LSCF displays a higher degradation rate than $La_{1-x}Sr_xMnO_3$ (LSM) cathodes, attributed to Sr segregation near surfaces or interfaces,[13,14] caused by electrostatic attraction of the negatively charged A-site dopants near the positively charged oxygen vacancies enriched at the surface.[15] The Sr-enriched phases (such as SrO islands on the surface) are detrimental to the surface activity, and also promote the formation and growth of other detrimental secondary phases (*e.g.*, $SrCO_3$, $Sr(OH)_2$, $SrCrO_4$, *etc.*), leading to time-dependent degradation in performance.[16] One possible solution is to develop new cathode materials or architectures which are resistant against Sr-segregation. For example, Sr-free cathode materials have been extensively studied. Perovskite or Ruddlesden–Popper (RP) perovskite-like materials, such as $La(Ni,Fe)O_{3-\delta}$, Nd_2NiO_4 and Pr_2NiO_4, were thus proposed and studied as candidate SOFC cathode materials.[17,18] To date, unfortunately, none of the new cathode materials have all the desired properties: high ORR activity, suitable compatibility with other cell components (*e.g.*, electrolyte and interconnects), and sufficient durability under realistic operating conditions.

Surface modifications with catalytically-active nanoparticles have been widely used in chemical and electro-catalytic catalysis[19,20] and SOFCs.[21] However, discrete particles may have limited effect on suppressing Sr segregation.[22] Recently, conformal perovskite coatings (*e.g.* $La_{0.85}Sr_{0.15}MnO_3$) have been deposited on LSCF surfaces to enhance performance and stability.[10,23] When the crystal structure of the catalyst is similar to that of LSCF, the catalyst coating can be conformal and dense to effectively suppress Sr segregation and enhance the durability of the cathode.[24] For a catalyst-coated LSCF electrode, the porous LSCF backbone serves as a "highway" for facile transport of both oxygen ions and electrons (or electron holes) while the thin catalyst coating offers enhanced ORR activity and durability.[25] The desired catalyst layer should be conformal, highly active for ORR, and inert to contaminants encountered under realistic operating conditions.

Here, we report our findings in dramatically enhancing both the ORR kinetics and stability of the state-of-the-art LSCF cathode by applying a conformal coating of a hybrid catalyst derived from a one-step infiltration process.[26] The hybrid catalyst is composed of a conformal film of the perovskite $PrNi_{0.5}Mn_{0.5}O_3$ (PNM) and exsoluted PrO_x nanoparticles. Analyses suggest that the PrO_x nanoparticles dramatically enhance the ORR kinetics *via* a high concentration of oxygen vacancies while the thin PNM film effectively suppresses Sr segregation from the LSCF phase, thus significantly enhancing the stability of the cathode.

Results and discussion

RP-type layered perovskite, $Pr_2NiO_{4+\delta}$ (δ = 0.15–0.22), has been studied as a potential cathode for SOFCs because of its unique oxygen ion transport properties.[17,18] When a Mn-doped $Pr_2NiO_{4+\delta}$ with an intended formula of $Pr_2Ni_{0.5}Mn_{0.5}O_{4+\delta}$ was used as a catalyst to coat the surface of a porous LSCF cathode, however, it was found that the catalyst layer is, in fact, composed of a PrO_x phase (with a possible composition of Pr_7O_{12}) and a single perovskite phase $PrNi_{0.5}Mn_{0.5}O_3$ (PNM) (ESI,† Fig. S1) under the conditions of our study (solution infiltration of catalysts into a porous LSCF cathode). The advantages of the nanoparticles derived from an exsolution process over those from other deposition techniques (such as solution infiltration of nanoparticles[27,28]) include better control over particle size, distribution, and morphological stability. To probe the surface chemistry and electronic structure of the hybrid catalyst in order to explain the mechanism of performance enhancement, we deposited a thin-film of the catalyst on a model cell with a flat, dense LSCF electrode using pulsed laser deposition (PLD) (ESI,† Fig. S2 and S3). The similarity in the crystal structure of PNM to that of LSCF facilitates facile epitaxial growth of a dense and conformal coating of PNM on each LSCF grain (ESI,† Fig. S4), allowing us to evaluate its effect on suppressing Sr segregation and, thus, on enhancing the stability and durability of the LSCF cathode.[10]

The unique architecture of the catalyst-coated electrode

Fig. 1a schematically shows the surface morphology of a hybrid catalyst coating on a porous LSCF electrode backbone (sintered large LSCF grains); the conformal coating is composed of a PNM film decorated with PrO_x nanoparticles. Fig. 1b shows a TEM image of two PrO_x particles on the PNM coating. The two insets in Fig. 1b are the Fast Fourier Transform (FFT) patterns of the PrO_x nanoparticles (fluorite structure) and the PNM coating (perovskite structure), respectively (see the ESI,† Fig. S4a and b). The FFT pattern of the nanoparticles (inset of Fig. 1b), together with the Electron Energy Loss Spectroscopy (EELS) spectra shown in Fig. 1b acquired from two locations (1 and 2 in b) further indicated that these nanoparticles are mainly PrO_x. The superlattice spots in the FFT pattern (location 1) are induced most likely by the formation of oxygen vacancies ordering within PrO_x.[29,30] Shown in Fig. 1c is a cross-sectional view (a high-angle annular dark field STEM image) of the hybrid catalyst coated LSCF. The EELS spectra (Fig. 1d) acquired along the red line marked on Fig. 1c clearly indicated that the exsoluted particles are PrO_x while the thin PNM layer ($\sim$10 nm thick) was conformally coated on the LSCF surface.

Electrochemical performance

Shown in Fig. 2a are some typical electrochemical impedance spectra (EIS), acquired in ambient air at 750 °C under open circuit voltage (OCV) conditions, of the symmetrical cells with bare LSCF, PNM-coated LSCF, PrO_x-coated LSCF, and the hybrid catalyst (PNM and PrO_x)-coated LSCF electrodes (ESI,† Fig. S5a and b). The R_p values at 750 °C of these electrodes are 0.134, 0.068, 0.030, and 0.022 Ω cm^2 for bare LSCF, PNM-coated LSCF, PrO_x-coated LSCF, and the hybrid-catalyst-coated LSCF, respectively. Clearly, the LSCF coated with a thin film of the hybrid catalyst (PNM and PrO_x) displayed the lowest R_p among all cathodes studied, much better than the other two excellent cathodes reported earlier: $La_{0.4875}Ca_{0.0125}Ce_{0.5}O_{2-\delta}$ (LCC) coated-LSCF[31] and $PrSrCoMnO_{6-\delta}$ (PSCM) coated-LSCF[23] (ESI,† Fig. S6). The results

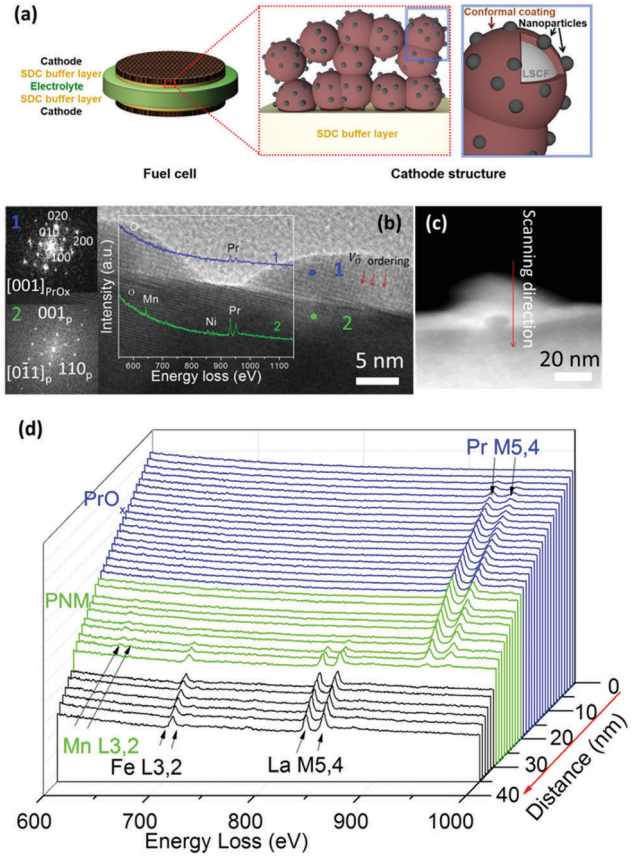

Fig. 1 (a) Schematics of an LSCF electrode backbone decorated with a conformal, dense PNM coating and exsoluted PrO_x nanoparticles. (b) A high-resolution TEM image showing two PrO_x particles on a conformal PNM coating deposited on an LSCF grain. The insets are the FFT patterns from the nanoparticles (point 1) and the conformal PNM coatings (point 2); and the EELS spectra from point 1 and 2, suggesting that the nanoparticles are mainly PrO_x (point 1) while the conformal coating is PNM (point 2). (c) High-angle annular dark field (HAADF) STEM image of a cross-section of the hybrid catalyst-coated LSCF cathode. (d) EELS spectra acquired along the red line marked in (c), indicating that the exsoluted particles are PrO_x whereas the thin, conformal coating is PNM on the top of the LSCF grain.

suggest that the hybrid catalyst (PNM and PrO_x) has the highest ORR activity on LSCF. Further, the surface exchange kinetics of these cathodes was also determined from electrical conductivity relaxation (ECR) measurements (Fig. 2b and ESI,† Fig. S7). At 750 °C, the surface exchange coefficient (k) for the bare LSCF was $\sim 5.68 \times 10^{-4}$ cm s^{-1}, which is consistent with previous values reported for LSCF.[32–34] The k for PrO_x-, PNM- and hybrid catalyst coated LSCF electrodes increased to $\sim 1.77 \times 10^{-2}$, 7.58×10^{-3}, and 7.50×10^{-3} cm s^{-1}. The highest k of the PrO_x-LSCF electrode may suggest that PrO_x is most active for oxygen exchange; however, the hybrid catalyst-coated LSCF electrode showed the lowest R_p in the symmetrical cell, suggesting that the overall rate of the cathode processes depends also on other factors such as the rate of ionic transport associated with the ORR. The conformal coating of PNM plays a vital role in facilitating rapid oxygen-ion transport into LSCF, as to be elaborated later.

Shown in Fig. 2c are typical I–V–P curves of anode-supported cells (ESI,† Fig. S5c) based on bare or catalyst-coated LSCF cathodes at 750 °C. A peak power density (P_{max}) of 1.21 W cm^{-2} was achieved for the cell with a hybrid PNM–PrO_x catalyst coated LSCF, much higher than 1.09 W cm^{-2} for PrO_x-LSCF, 0.88 W cm^{-2} for PNM-LSCF, and 0.79 W cm^{-2} for bare LSCF. Shown in Fig. 2d are the power densities of the anode-supported cells with different cathodes operated at 750 °C under a constant cell voltage of 0.7 V for ~500 h. Clearly, the cell having a hybrid catalyst coated LSCF electrode showed not only the highest power density but also the best durability. It is noted that the surface morphology/composition had slightly changed during the initial 110 h of testing; more PrO_x particles were exsolved from the parent coating, leading to some improvement in performance during this period of time (ESI,† Fig. S8a and b). After ~110 h of operation, however, the morphology became reasonably stable; the subsequent durability in performance is attributed to the observed stability in morphology, composition, and structure of the hybrid catalyst coated LSCF electrodes (ESI,† Fig. S8c, d and S9–S11).

The origin of performance and stability enhancement

It is most likely that the two phases of the hybrid catalyst, PrO_x and PNM, contributed synergetically to the ORR activity and the durability of the cathodes. Oxygen can be readily incorporated through highly active PrO_x particles. The cells with PNM coating showed an initially lower performance (compared with the PrO_x coating and hybrid catalyst coating) but a significant activation behavior over time. The hybrid catalyst coated-LSCF shows the lowest R_p, highest power output, and best stability among the cathode combinations studied, suggesting that the PrO_x nanoparticles dramatically facilitate the ORR kinetics, while the conformal thin PNM film enhances the stability. In order to test this hypothesis, we probed the surface electronic structure and composition of the bare LSCF (~100 nm), and PNM-, PrO_x- and hybrid catalyst (~10 nm)-coated LSCF (~100 nm) thin-film model electrode systems using Near Ambient Pressure XPS and NEXAFS.

Fast ORR kinetics: surface oxygen vacancies and charge transfer ability on PrO_x. The electron transfer from the cathode surface to the oxygen molecule is an important step for the ORR. The density of states (DOS) near the Fermi level (E_F) is a simple descriptor used for characterizing the easiness of electron transfer.[35,36] The X-ray photo electron spectra of the valence band (VB) provide information about the filled states (Fig. 3a). The VB structures near the Fermi level for bare LSCF, and PNM-, PrO_x-, and hybrid catalyst-coated LSCF are shown in Fig. 3b. Since the area of the VB spectra of all the samples was normalized to one, the intensity of the spectra represents the DOS in the VB. The DOS at E_F for PrO_x-LSCF and hybrid-LSCF was higher than those for either bare LSCF or PNM-LSCF (Fig. 3b), indicating easier charge transfer from the PrO_x-LSCF and hybrid-LSCF surface to absorbed oxygen molecules.[35,36]

For SOFC cathodes, the concentration of oxygen vacancies is also a decisive factor for fast oxygen exchanges.[37–40] The change in the X-ray absorption spectra (XAS) and the intensity near the E_F in the VB spectra as a function of temperature indicated that oxygen vacancies are readily formed in PrO_x at elevated temperature, suggesting that PrO_x nanoparticles are likely the active phase for ORR in the hybrid catalyst-coated-LSCF cathodes.

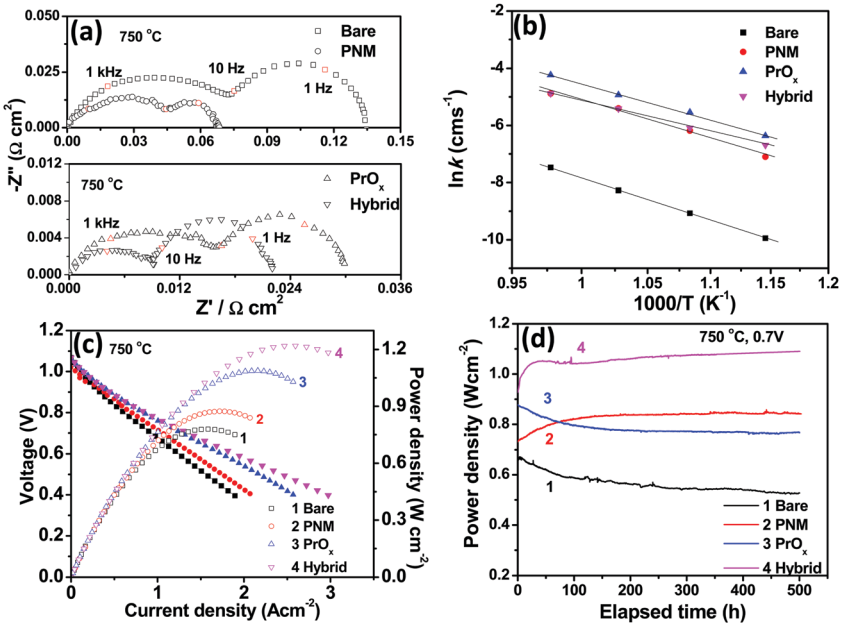

Fig. 2 (a) Typical electrochemical impedance spectra of cells with a bare LSCF, and PNM-, PrO_x- and hybrid catalyst-coated LSCF electrode, measured in ambient air at 750 °C under OCV conditions; (b) temperature dependence of the surface exchange coefficient (k) of the bare LSCF and catalyst-coated LSCF cathodes; (c) typical I–V–P curves and (d) stability testing (at a constant cell voltage of 0.7 V) for Ni–YSZ anode supported cells with a bare LSCF or PNM-, PrO_x- or hybrid PNM–PrO_x catalyst-coated LSCF cathode at 750 °C using 3% humidified H_2 as fuel and ambient air as the oxidant.

The NEXAFS probes the unfilled electronic states. For bare LSCF, the feature i in the O K-edge XAS (Fig. 3c) is attributed to the unoccupied states of the O 2p-transition metal (TM) 3d hybridization band. With increasing temperature, more oxygen vacancies form at the LSCF surface, leading to the population of electronic states near the Fermi level, and so the e_g absorption feature (red arrow) intensity decreases.[41,42] The t_{2g} absorption feature (black arrow) slightly increases, which is attributed to a change in the degree of covalency.[41,42] From the transition metal (TM) L-edge XAS, a slight reduction in the Co valence state was observed, while the Fe valence state remained the same (ESI,† Fig. S12). For PrO_x-LSCF, the O K-edge XAS (Fig. 3c) is similar to that of the cubic PrO_x,[43,44] consistent with the cubic structure of PrO_x quantified by XRD (ESI,† Fig. S3 and S4). Similar to LSCF, the intensity of the feature i in the O K-edge XAS of the PrO_x-LSCF, corresponding to the Pr 4f–O 2p hybridization band, decreased significantly with temperature. Such a decrease is likely due to the formation of oxygen vacancies, which leave excess electrons filling into the unoccupied Pr 4f–O 2p band. The change in the O K-edge XAS of the hybrid PNM–PrO_x catalyst coated-LSCF followed the same trend as that on the PrO_x-coated LSCF. The PNM-LSCF, on the other hand, did not show any detectable change in the O K edge XAS.

Consistent with the change in the O K edge XAS above, with increasing temperature the intensity near the Fermi level in the VB spectra of the PrO_x-LSCF increases and the top of the VB shifts up towards the Fermi level (Fig. 3b). Such a change is likely due to the formation of oxygen vacancies in the PrO_x-LSCF at high temperature, leading to creation of states near the Fermi level. The VB of the hybrid PNM–PrO_x coated LSCF followed the behavior of the VB of the PrO_x-LSCF, while the shift in the VB top is less on PNM-LSCF (Fig. 3b). Furthermore, both the Ni and Mn L edge spectra for the hybrid catalyst (Fig. 3d and e) did not show any noticeable variation with temperature, indicating no change in the Ni and Mn valence states. All these results indicate that the temperature-dependent changes of the VB structure and the O K-edge XAS of the hybrid PNM–PrO_x catalyst with temperature arises from the formation of oxygen vacancies in PrO_x. Based on oxygen vacancy availability as deduced from our XPS and XAS measurements, the PrO_x is the active phase on the hybrid catalyst coated LSCF surface for a fast oxygen exchange process.

Enhanced durability: inherent chemical stability of the hybrid coating. To understand the mechanism for high stability of the hybrid PNM–PrO_x catalyst-coated LSCF, we investigated the surface chemistry of LSCF, the hybrid catalyst, and the hybrid catalyst coated LSCF model thin films exposed to reactive gas (O_2, H_2O) at elevated temperatures. All samples were first cleaned from carbon in 200 mTorr O_2 at 300 °C, and then heated to 500 °C in O_2. Subsequently, 10% H_2O was added to the O_2 gas environment while the temperature was kept at 500 °C. Shown in Fig. 4 are the (La + Sr)/(Co + Fe) ratio for LSCF (quantified from La 3d, Sr 3d, Co 2p and Fe 2p peak area) and the Pr/(Ni + Mn) ratio for the hybrid catalyst (quantified from Pr 4d, Ni 3p and Mn 3p) as a function of measurement conditions. Clearly, the (La + Sr)/(Co + Fe) ratio of LSCF increased significantly as the temperature was increased from 300 to 500 °C in O_2 or when 10% H_2O was introduced at 500 °C. In contrast, the Pr/(Ni + Mn) ratio of the hybrid catalyst varied only slightly under similar conditions. Furthermore, the LSCF surface became much rougher by forming large precipitate particles accompanying the large increase in (La + Sr)/(Co + Fe) ratio of LSCF. In contrast, the surface morphology of the hybrid catalyst stayed nearly unchanged

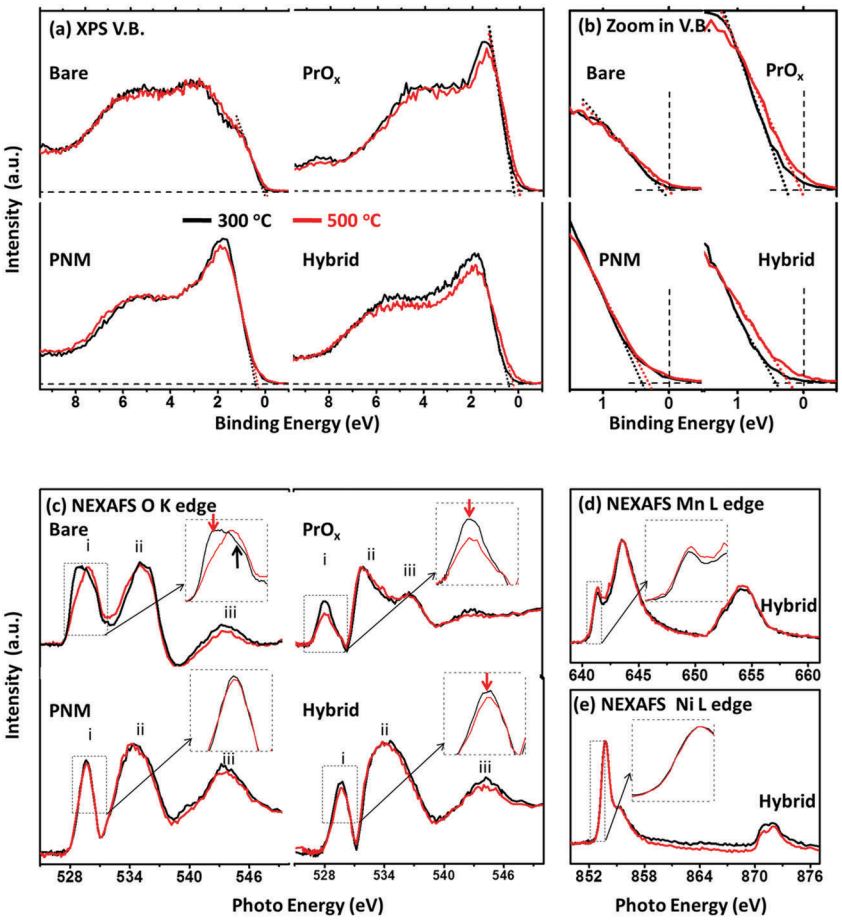

Fig. 3 Surface electronic structure of bare LSCF, and PNM-, PrO_x-, and hybrid catalyst (PNM–PrO_x)-coated-LSCF model thin films characterized using near ambient XPS and NEXAFS at 300 °C (black line) and 500 °C (red line) in a 200 mTorr O_2 environment. (a) XPS valence band structure of different films. The area of all the valence spectra was normalized to unity. (b) Zoomed in valence band spectra near the Fermi level region. The black and red dotted lines are the linear fittings of the valence band edge, and the black dash lines mark the zero intensity and binding energy position. (c) The O K-edge absorption spectra of bare LSCF, and PNM-, PrO_x-, and hybrid catalyst-coated LSCF. Three features in the LSCF O K-edge spectra are attributed to the unoccupied state of hybrid transition metal TM(Co,Fe) d–O 2p band (feature i); La 5d/Sr 4d–O 2p states (feature ii) and Co and Fe sp–O 2p hybridized bands (feature iii).[41,42,45,46] The insets in (c) are zoomed-in views of the pre-edge region. (d) Mn L-edge and (e) Ni L-edge absorption spectra of the hybrid catalyst (PNM–PrO_x).

(ESI,† Fig. S13). All these results prove that the hybrid catalyst surface is more stable chemically than LSCF when exposed to the gases relevant to SOFC operation at high temperatures. The O 1s, Sr 3d and Pr 4d photoelectron spectra provide further evidence to support that the hybrid catalyst has better stability than LSCF (ESI,† Fig. S14 and S15).

Mechanism of ORR acceleration probed by computation

Periodic density functional theory (DFT) simulations were performed to gain more insight into the mechanism of the enhanced ORR and stability on the hybrid catalyst coating, by examining oxygen adsorption, vacancy formation and oxygen transport processes. As will be seen below, the strong oxygen adsorption and easier vacancy formation predicted by DFT calculations here are consistent with the results obtained from XPS and XAS above. Furthermore, fast oxygen transport due to exsoluted PrO_x particles and a more stable surface due to the conformal PNM coating can be expected based on these calculations, the latter also being consistent with the XPS results above.

We calculated the oxygen adsorption energy on PrO_2 and oxygen vacancy formation energy in PrO_2 using PBE + U,[47] and we took CeO_2 as an excellent model catalyst reference for comparison. Shown in ESI,† Table S1 are the calculated oxygen vacancy formation energies (E_{V_O}) for bulk PrO_2 and CeO_2 (1.04 eV and 4.69 eV, respectively) and the adsorption energy of O_2 on the PrO_2(111) and CeO_2(111) surfaces (−1.19 and ~0.00 eV, respectively) with an end-on configuration. These quantities are characteristic of how fast the surface oxygen exchange and bulk oxygen diffusion kinetics are.[48] In comparison to CeO_2, the stronger O_2 adsorption and much lower oxygen vacancy formation energy (E_{V_O}) of PrO_2 support the ease of oxygen uptake and the exceptional ORR kinetics on the PrO_2 surface under the cathodic conditions. The strong adsorption of oxygen molecule (presumably as chemisorption) on PrO_x is consistent with the easier charge transfer found on PrO_x by XAS and XPS above. The calculated E_{V_O} for PrO_x (1.04 eV) is much

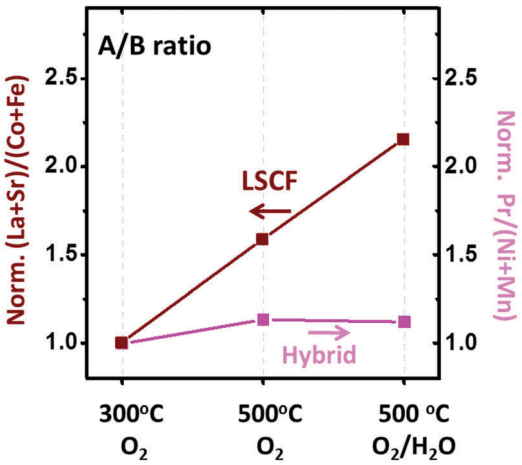

Fig. 4 Surface composition of LSCF and the hybrid catalyst (PNM–PrO_x) measured under different conditions: 200 mTorr of O_2 at 300 °C, 200 mTorr of O_2 at 500 °C, and 200 mTorr of a gas mixture (90% O_2 + 10% H_2O) at 500 °C. For comparison, the (La + Sr)/(Co + Fe) and Pr/(Ni + Mn) were normalized by the values obtained in 200 mTorr of O_2 at 300 °C.

smaller than that of PNM (3.63 eV) and LSCF (2.38 eV) (ESI,† Table S2). This is also consistent with the larger amount of oxygen vacancies found in PrO_x from the XPS and XAS measurements above.

Furthermore, a localized oxygen vacancy transport channel could be formed in the thin-film PNM phase during the PrO_x exsolution process, allowing for fast oxygen transport through the PrO_x/PNM-LSCF electrode system. Localized growth of PrO_x nanoparticles (Fig. 2) may inevitably result in local Pr deficiency in the parent PNM coating. Migration barriers for oxygen diffusion were calculated to understand the effect of Pr deficiency in the PNM bulk phase, similar to a previous study.[48] The stoichiometric bulk PNM structure has a migration barrier (E_m) of 1.26 eV, while the structure with Pr deficiency has a much lower barrier of 0.45 eV (ESI,† Table S3). More interestingly, the non-stoichiometric structure shows a smoothly curved vacancy trajectory, while the stoichiometric structure has a strong interaction between the vacancy and the neighboring ions (Fig. 5a and b). The bulk diffusion barrier E_a is the summation of the migration barrier (E_m) and oxygen vacancy formation energy (E_{V_O}), as compiled in ESI,† Table S3. In effect, in this system the bulk diffusion barrier was lowered from 4.89 eV to 1.62 eV due to Pr deficiency (ESI,† Fig. S16). The 67% lowering of the bulk diffusion barrier in Pr-deficient PNM supports the possibility of fast oxygen transport through the thin PNM layer. In addition, we examined the migration energy of oxygen from the PrO_x surface into the Pr-deficient PNM subsurface. To simplify the problem, we assessed the PrO_x-terminated surface of PNM to represent the oxygen transfer from PrO_x particles into PNM. The surface energy calculations show that PrO-terminated surfaces are more stable than Ni and Mn-terminated ones. As shown in ESI,† Fig. S17, for the configuration without Pr deficiency in PNM, a 0.21 eV barrier is required to diffuse into the sub-surface, followed by overcoming a migration barrier of 0.93 eV to reach the oxygen vacancy. However, for the case with Pr deficiency in the PNM, oxygen is instantaneously incorporated into the sub-surface without a barrier, and then it hops by overcoming a 0.82 eV barrier. The 12% reduction in the migration barrier and the non-existence of the incorporation barrier clearly manifests that Pr deficiency in PNM could be a critical factor in enhancing the oxygen transport into and through the bulk layers. Overall, on the basis of the surface and bulk calculations, the enhanced ORR and fast bulk diffusion of the hybrid catalyst coated LSCF cathode is illustrated in Fig. 5c. Gas-phase oxygen adsorbs either preferentially on PrO_x nanoparticles or on the PrO_x-terminated surfaces of PNM, followed by dissociation. Subsequently, monoatomic oxygen diffuses through the PrO_x surface or the

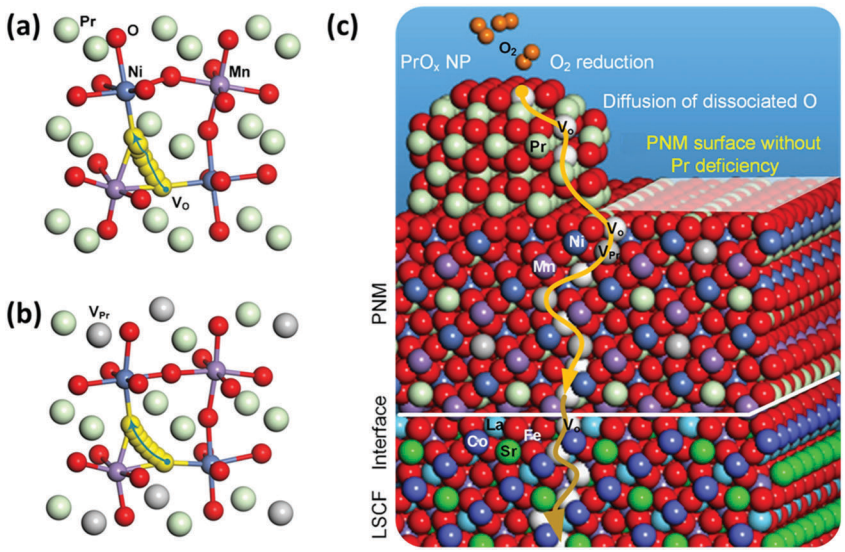

Fig. 5 Schematic representation of a trajectory of oxygen vacancies (a) without and (b) with Pr deficiency (V_{Pr}). The solid arrow represents the oxygen migration trajectory. (c) Schematic representation of the lowest energy pathway for the O_2 reduction on the hybrid catalyst (PrO_x/PNM) coated LSCF cathode and the enhanced bulk diffusion of oxygen vacancies in PNM by introducing Pr deficiency.

PrO_x bulk, migrating down into PNM and to the cathode/electrolyte interface.

Finally, the lattice mismatch between PNM and LSCF is only 0.4%, allowing the formation of a conformal PNM coating on LSCF (as shown in Fig. 1c), and the PNM layer protects the surface against chemical degradation. The segregation and phase precipitation of the A-site elements (*e.g.*, Sr) are well accepted in the literature to be detrimental to the performance of LSCF and perovskite-related materials.[49,50] Indeed, the continuous degradation in LSCF performance (Fig. 2d) is attributed to Sr segregation on LSCF as shown in Fig. 4. One driving force for Sr segregation is the net positive charge at the surface due to the preferential formation of oxygen vacancies.[15] The coverage by a conformal hybrid catalyst layer with high oxygen vacancy formation energy (ESI,† Table S2) can suppress the oxygen vacancy concentration at the LSCF/PNM interface, and in turn decrease the driving force for Sr segregation.[22] Consistent with this argument, the hybrid catalyst surface was found to be much more stable than the LSCF surface, both electrochemically (Fig. 2) and chemically (Fig. 4) when exposed to reactive gases at high temperatures.

Conclusions

In summary, both the ORR activity and the stability of the state-of-the-art LSCF cathode have been effectively enhanced through surface modification by an electrocatalytically active and robust hybrid catalyst coating composed of a conformal PNM film and exsoluted PrO_x nanoparticles. The dispersed PrO_x nanoparticles significantly accelerate the ORR kinetics because of the easier electron transfer and a larger concentration of oxygen vacancies at the surface. The inherently more stable PNM film greatly enhances the durability of the cathode by suppressing Sr segregation from LSCF. The combination of distinctive properties of the two separate phases, together with their unique morphology and architecture, provide a dramatic enhancement in electrocatalytic performance and long-term durability of a state-of-the-art electrode backbone. The process involves a simple, one-step surface modification. The demonstrated approach of surface enhancement is attractive not only for intermediate-temperature SOFCs, but also for other types of energy conversion and storage systems, including electrolysis cells for hydrogen production and membrane reactors for the synthesis of clean fuels.

Experimental

Methods and any associated references are available in the ESI.†

Author contributions

M. L. and B. Y. conceived, designed and supervised the project. Yu C., Yan C., and D. D. contributed equally to this work. Yu C. and D. D. carried out the fabrication of the samples and conducted data analysis of all electrochemical experiments. B. Z. and S. Y. performed the electrical conductivity relaxation measurement. D. C. performed the Raman analysis. Yan C., Q. L., H. B., E. C., G. V., and J. W. fabricated the PLD films and characterized the surface chemistry of the thin films. YongMan C. and L. Z. conducted the DFT calculation. Yu C., H. X, and Y. D. conducted TEM analysis. B. Z., C. Y., and J. L. collected the data of X-ray diffraction and SEM. Yu C. and B. D. performed the XPS analysis of the cathodes. Yu C., Yan C., YongMan C., M. L., and B. Y. contributed to writing the paper.

Acknowledgements

This work was supported by the US Department of Energy SECA Core Technology Program (DE-NT0006557), DOE ARPA-E REBELS Program (DE-AR0000502), and Guangdong Innovative and Entrepreneurial Research Team Program (No. 2014ZT05N200). B. Y. and Yan. C. acknowledge financial support for this research from the DoE Basic Energy Sciences (DE-SC0002633), and Yan. C. acknowledges fellowship financial support from the Schlumberger Foundation for Faculty of the Future Program. This research used resources of the National Energy Research Scientific Computing Center, a DOE Office of Science User Facility supported by the Office of Science of the U.S. Department of Energy under Contract No. DE-AC02-05CH11231. This research also used the Advanced Light Source that is supported by the Director, Office of Science, Office of Basic Energy Sciences, of the U.S. Department of Energy under Contract No. DE-AC02-05CH11231. We thank Dr Sean Bishop and Dr Nikolai Tsvetkov for the assistance with XPS and NEXAFS experiments.

References

1 E. D. Wachsman and K. T. Lee, *Science*, 2011, **334**, 935–939.
2 Z. Zhan and S. A. Barnett, *Science*, 2005, **308**, 844–847.
3 Z. Shao and S. M. Haile, *Nature*, 2004, **431**, 170–173.
4 E. P. Murray, T. Tsai and S. A. Barnett, *Nature*, 1999, **400**, 649–651.
5 L. Carrette, K. A. Friedrich and U. Stimming, *Fuel Cells*, 2001, **1**, 5–39.
6 L. Yang, S. Wang, K. Blinn, M. Liu, Z. Liu, Z. Cheng and M. Liu, *Science*, 2009, **326**, 126–129.
7 L. Yang, Y. Choi, W. Qin, H. Chen, K. Blinn, M. Liu, P. Liu, J. Bai, T. A. Tyson and M. Liu, *Nat. Commun.*, 2011, **2**, 357.
8 Y. Chen, Y. Zhang, Y. Lin, Z. Yang, D. Su, M. Han and F. Chen, *Nano Energy*, 2014, **10**, 1–9.
9 B. C. H. Steele and A. Heinzel, *Nature*, 2001, **414**, 345–352.
10 M. E. Lynch, L. Yang, W. Qin, J.-J. Choi, M. Liu, K. Blinn and M. Liu, *Energy Environ. Sci.*, 2011, **4**, 2249–2258.
11 Y. Chen, Y. Lin, Y. Zhang, S. Wang, D. Su, Z. Yang, M. Han and F. Chen, *Nano Energy*, 2014, **8**, 25–33.
12 Y. Chen, Y. Bu, Y. Zhang, R. Yan, D. Ding, B. Zhao, S. Yoo, D. Dang, R. Hu, C. Yang and M. Liu, *Adv. Energy Mater.*, 2016, DOI: 10.1002/aenm.201601890.
13 S. P. Jiang and X. Chen, *Int. J. Hydrogen Energy*, 2014, **39**, 505–531.
14 S. P. Simner, M. D. Anderson, M. H. Engelhard and J. W. Stevenson, *Electrochem. Solid-State Lett.*, 2006, **9**, A478–A481.

15 W. Lee, J. W. Han, Y. Chen, Z. Cai and B. Yildiz, *J. Am. Chem. Soc.*, 2013, **135**, 7909–7925.
16 S. P. Jiang, S. Zhang and Y. D. Zhen, *J. Electrochem. Soc.*, 2006, **153**, A127–A134.
17 T. Komatsu, H. Arai, R. Chiba, K. Nozawa, M. Arakawa and K. Sato, *Electrochem. Solid-State Lett.*, 2006, **9**, A9–A12.
18 X. D. Zhou, J. W. Templeton, Z. Nie, H. Chen, J. W. Stevenson and L. R. Pederson, *Electrochim. Acta*, 2012, **71**, 44–49.
19 Y. Nishihata, J. Mizuki, T. Akao, H. Tanaka, M. Uenishi, M. Kimura, T. Okamoto and N. Hamada, *Nature*, 2002, **418**, 164–167.
20 R. J. Gorte and J. M. Vohs, *Curr. Opin. Colloid Interface Sci.*, 2009, **14**, 236–244.
21 Z. Jiang, C. Xia and F. Chen, *Electrochim. Acta*, 2010, **55**, 3595–3605.
22 N. Tsvetkov, Q. Lu, L. Sun, E. J. Crumlin and B. Yildiz, *Nat. Mater.*, 2016, **15**, 1010–1017.
23 D. Ding, M. Liu, Z. Liu, X. Li, K. Blinn, X. Zhu and M. Liu, *Adv. Energy Mater.*, 2013, **3**, 1149–1154.
24 H. Ding, A. V. Virkar, M. Liu and F. Liu, *Phys. Chem. Chem. Phys.*, 2013, **15**, 489–496.
25 D. Ding, X. Li, S. Y. Lai, K. Gerdes and M. Liu, *Energy Environ. Sci.*, 2014, **7**, 552–575.
26 D. Ding and M. Liu, Electrocatalytic conformal coatings and method for making the same, *US Pat.*, US 20150325860 A1, 2015.
27 D. Neagu, G. Tsekouras, D. N. Miller, H. Ménard and J. T. S. Irvine, *Nat. Chem.*, 2013, **5**, 916–923.
28 D. E. Fowler, A. C. Messner, E. C. Miller, B. W. Slone, S. A. Barnett and K. R. Poeppelmeier, *Chem. Mater.*, 2015, **27**, 3683–3693.
29 D. R. Ou, T. Mori, F. Ye, T. Kobayashi, J. Zou, G. Auchterlonie and J. Drennan, *Appl. Phys. Lett.*, 2006, **89**, 171911.
30 Y. Ding, Y. Chen, K. C. Pradel, M. Liu and Z. Lin Wang, *J. Appl. Phys.*, 2016, **120**, 214302.
31 M. Liu, D. Ding, K. Blinn, X. Li, L. Nie and M. Liu, *Int. J. Hydrogen Energy*, 2012, **37**, 8613–8620.
32 R. A. Cox-Galhotra and S. McIntosh, *Solid State Ionics*, 2010, **181**, 1429–1436.
33 L. Zhao, J. Hyodo, K. Chen, N. Ai, S. Amarasinghe, T. Ishihara and S. P. Jiang, *J. Electrochem. Soc.*, 2013, **160**, F682–F686.
34 J. Lane and J. Kilner, *Solid State Ionics*, 2000, **136**, 997–1001.
35 Z. H. Cai, Y. Kuru, J. W. Han, Y. Chen and B. Yildiz, *J. Am. Chem. Soc.*, 2011, **133**, 17696–17704.
36 P. J. Feibelman and D. R. Hamann, *Phys. Rev. Lett.*, 1984, **52**, 61–64.
37 M. Pavone, A. M. Ritzmann and E. A. Carter, *Energy Environ. Sci.*, 2011, **4**, 4933–4937.
38 Y.-L. Lee, D. Lee, X. R. Wang, H. N. Lee, D. Morgan and Y. Shao-Horn, *J. Phys. Chem. Lett.*, 2016, **7**, 244–249.
39 Y. L. Lee, J. Kleis, J. Rossmeisl, Y. Shao-Horn and D. Morgan, *Energy Environ. Sci.*, 2011, **4**, 3966–3970.
40 Z. A. Feng, F. El Gabaly, X. Ye, Z.-X. Shen and W. C. Chueh, *Nat. Commun.*, 2014, **5**, 4374.
41 Y. Orikasa, T. Ina, T. Nakao, A. Mineshige, K. Amezawa, M. Oishi, H. Arai, Z. Ogumi and Y. Uchimoto, *Phys. Chem. Chem. Phys.*, 2011, **13**, 16637–16643.
42 D. N. Mueller, M. L. Machala, H. Bluhm and W. C. Chueh, *Nat. Commun.*, 2015, **6**, 6097.
43 O. Seifarth, J. Dabrowski, P. Zaumseil, S. Mueller, D. Schmeisser, H. J. Muessig and T. Schroeder, *J. Vac. Sci. Technol., B: Microelectron. Nanometer Struct.–Process., Meas., Phenom.*, 2009, **27**, 271–276.
44 A. Schaefer, V. Zielasek, T. Schmidt, A. Sandell, M. Schowalter, O. Seifarth, L. E. Walle, C. Schulz, J. Wollschlager, T. Schroeder, A. Rosenauer, J. Falta and M. Baumer, *Phys. Rev. B*, 2009, **80**, 045414.
45 M. Abbate, F. M. F. Degroot, J. C. Fuggle, A. Fujimori, O. Strebel, F. Lopez, M. Domke, G. Kaindl, G. A. Sawatzky, M. Takano, Y. Takeda, H. Eisaki and S. Uchida, *Phys. Rev. B*, 1992, **46**, 4511–4519.
46 T. Mizokawa, A. Fujimori, T. Arima, Y. Tokura, N. Mori and J. Akimitsu, *Phys. Rev. B: Condens. Matter Mater. Phys.*, 1995, **52**, 13865–13873.
47 Y. Choi, M. C. Lin and M. Liu, *Angew. Chem., Int. Ed.*, 2007, **46**, 7214–7219.
48 Y. Choi, M. C. Lin and M. Liu, *J. Power Sources*, 2010, **195**, 1441–1445.
49 Y. Chen, W. C. Jung, Z. Cai, J. J. Kim, H. Tuller and B. Yildiz, *Energy Environ. Sci.*, 2012, **5**, 7979–7988.
50 J. W. Han and B. Yildiz, *Energy Environ. Sci.*, 2012, **5**, 8598–8607.

